# Acetobacter turbidans α-Amino Acid Ester Hydrolase. How a Single Mutation Improves an Antibiotic-Producing Enzyme

Barends, Thomas R.M.; Polderman-Tijmes, Jolanda J.; Jekel, Peter A.; Williams, Christopher; Wybenga, Gjalt; Janssen, Dick B.; Dijkstra, Bauke W.

*Published in:*
The Journal of Biological Chemistry

*DOI:*
10.1074/jbc.M511187200



*Publication date:*
2006

THE JOURNAL OF BIOLOGICAL CHEMISTRY VOL. 281, NO. 9, pp. 5804–5810, March 3, 2006


# *Acetobacter turbidans* α-Amino Acid Ester Hydrolase

## *HOW A SINGLE MUTATION IMPROVES AN ANTIBIOTIC-PRODUCING ENZYME**

Received for publication, October 14, 2005, and in revised form, November 21, 2005 Published, JBC Papers in Press, December 23, 2005, DOI 10.1074/jbc.M511187200

**Thomas R. M. Barends[‡], Jolanda J. Polderman-Tijmes[§], Peter A. Jekel[§], Christopher Williams[‡], Gjalt Wybenga[‡], Dick B. Janssen[§], and Bauke W. Dijkstra[‡1]**

*From the Laboratories of [‡]Biophysical Chemistry and [§]Biochemistry, University of Groningen, Nijenborgh 4, 9747 AG Groningen, The Netherlands*

**The α-amino acid ester hydrolase (AEH) from *Acetobacter turbidans* is a bacterial enzyme catalyzing the hydrolysis and synthesis of β-lactam antibiotics. The crystal structures of the native enzyme, both unliganded and in complex with the hydrolysis product D-phenylglycine are reported, as well as the structures of an inactive mutant (S205A) complexed with the substrate ampicillin, and an active site mutant (Y206A) with an increased tendency to catalyze antibiotic production rather than hydrolysis. The structure of the native enzyme shows an acyl binding pocket, in which D-phenylglycine binds, and an additional space that is large enough to accommodate the β-lactam moiety of an antibiotic. In the S205A mutant, ampicillin binds in this pocket in a non-productive manner, making extensive contacts with the side chain of $Tyr^{112}$, which also participates in oxyanion hole formation. In the Y206A mutant, the $Tyr^{112}$ side chain has moved with its hydroxyl group toward the catalytic serine. Because this changes the properties of the β-lactam binding site, this could explain the increased β-lactam transferase activity of this mutant.**

Thirty years ago, several bacterial strains, such as *Acetobacter turbidans* and *Xanthomonas citri*, were identified that were able to efficiently produce semi-synthetic β-lactam antibiotics from β-lactam nuclei produced by fermentation, and synthetic acyl compounds with an α-amino group (1). Important antibiotics with such acyl chains include cephalexin, cephadroxil, ampicillin, and amoxicillin. Given the difficulties in preparing such antibiotics by chemical means (2), much effort has been put into harnessing the β-lactam antibiotic synthesizing activity of these bacteria for application in the industrial production of antibiotics. It appeared that this activity originated from enzymes preferentially hydrolyzing esters of α-amino acids, the α-amino acid ester hydrolases (AEHs)[2] (3).

Because of its potential usefulness in antibiotic synthesis, the AEH from *A. turbidans* has been studied extensively, and it was the first of its family for which the gene was cloned and overexpressed (4). The sequence showed a G*X*S*Y*X*G* active site motif (4), which is characteristic of serine hydrolases of the X-prolyl dipeptidyl aminopeptidase family (5). Labeling studies with a suicide inhibitor, sequence alignments, and site-directed mutagenesis identified a catalytic triad of $Ser^{205}$, $Asp^{338}$, and $His^{370}$ in what was proposed to be a catalytic domain with an α/β-hydrolase fold (6).

Recently, the crystal structure of the *X. citri* AEH was solved (7). This enzyme shares 63% sequence identity with the *A. turbidans* AEH. The structure showed a tetrameric arrangement of monomers consisting of three domains each: an α/β-hydrolase domain at the N terminus, a helical cap domain, and a C-terminal jellyroll fold domain. The active site indeed contained a Ser-His-Asp catalytic triad, the constituents of which were found in their canonical positions in the α/β-hydrolase domain. Furthermore, a putative oxyanion hole was found in which a negative charge could be stabilized by a backbone amide and a tyrosine hydroxyl group. Similar folds and arrangements of active site residues were observed for the homologous cocaine esterase CocE (8) and *Lactococcus lactis* X-prolyl dipeptidyl aminopeptidase PepX (9). A particularly striking feature of the *Xanthomonas* AEH active site was a cluster of three carboxylate residues, which are conserved among the AEHs and were proposed to bind the positively charged α-amino group of the substrate from which the AEHs draw their name (7).

The coupling of acyl side chains to β-lactams by AEHs most likely proceeds through enzyme acylation at the catalytic serine residue by an acyl compound, followed by transfer of this acyl group to the amino group of an amino-β-lactam, through "aminolysis" of the acyl enzyme (3, 4, 10, 11). However, the acyl enzyme can also be hydrolyzed, and the synthesized antibiotic can also serve as substrate and be cleaved, as indicated in Fig. 1. Thus, the hydrolysis of the ester and the product occur as undesired side reactions (3, 11–13). Therefore, the AEH-catalyzed synthesis of antibiotics requires a kinetically controlled scheme. In such a scheme, the enzyme is added to a mixture of the acyl donor, *e.g.* D-phenylglycine methyl ester, and the acyl acceptor, *e.g.* 6-aminopenicillanic acid. All three reactions (synthesis of the antibiotic, hydrolysis of the ester, and hydrolysis of the antibiotic) will occur simultaneously, but after a certain period of time, a maximum in the antibiotic concentration is reached, at which time the reaction is stopped and the product harvested. The kinetic parameters of the enzyme govern the maximum level of antibiotic accumulation $P_S^{max}$ in such a process (14). Of crucial importance is the ratio of the specificity constants of the enzyme toward the acyl donor and the antibiotic, α, which is defined as $(k_{cat}/K_m)^{product}/(k_{cat}/K_m)^{acyl\ donor}$. For favorable antibiotic yield, α needs to be as small as possible. Another important factor is the ratio of the rates of synthesis and hydrolysis, measured as the ratio of the initial rates, $V_s/V_h^{ini}$. At a certain concentration of nucleophile, this ratio indicates the tendency of the acyl enzyme to undergo aminolysis rather than hydrolysis. For optimal antibiotic yield, $V_s/V_h^{ini}$ needs to be maximal (14, 15). Kinetic work has shown that mutation of $Tyr^{206}$ to alanine decreases the unwanted hydrolytic activity toward cephalexin in the *Acetobacter* enzyme (6). The corresponding residue in the *Xanthomonas* AEH was proposed to contribute to transition state stabilization with its main chain atoms (7).

* The costs of publication of this article were defrayed in part by the payment of page charges. This article must therefore be hereby marked "*advertisement*" in accordance with 18 U.S.C. Section 1734 solely to indicate this fact.

*The atomic coordinates and structure factors (codes 2B4K, 2B9V, 1NX9, and 1RYY) have been deposited in the Protein Data Bank, Research Collaboratory for Structural Bioinformatics, Rutgers University, New Brunswick, NJ (http://www.rcsb.org/).*

[1] To whom correspondence should be addressed. Tel.: 31-50-363-4381; Fax: 31-50-363-4800; E-mail: b.w.dijkstra@rug.nl.

[2] The abbreviations used are: AEH, α-amino acid ester hydrolase; D-PGM, D-phenylglycine methyl ester; WT, wild-type.

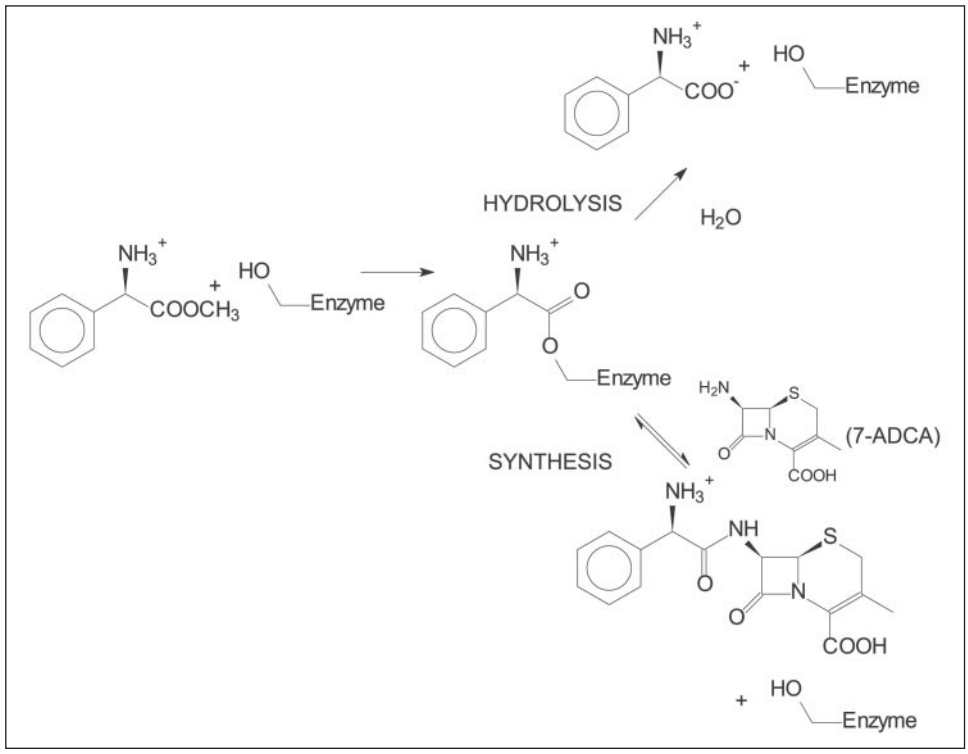


FIGURE 1. **Synthesis of antibiotics as catalyzed by AEHs.** The enzyme is acylated by an activated acyl compound, *e.g.* an ester. The resulting acyl enzyme can be hydrolyzed, resulting in a carboxylic acid. Alternatively, the acyl enzyme may be aminolyzed by an amino-β-lactam, resulting in the desired antibiotic. The partitioning between aminolysis and hydrolysis determines the $V_s/V_h^{ini}$. The product may also react with free enzyme to form acyl enzyme that can be hydrolyzed. The synthesis of cephalexin from D-phenylglycine methyl ester and 7-amino-desacetoxycephalosporanic acid is (*7-ADCA*) shown as an example.

The Y206A mutant of *Acetobacter* AEH was further investigated in terms of its usefulness as a biocatalyst for antibiotic production (16).

The present work reports the structure of the AEH from *A. turbidans*, aimed at understanding the precise mode of action of this enzyme. In addition to the native structure, the structures of the complex with D-phenylglycine, the Y206A mutant, and the inactive S205A mutant complexed with the antibiotic ampicillin are reported, as are the effects of the Y206A mutation on the kinetic parameters α, $V_s/V_h^{ini}$, and $P_S^{max}$. The structures give insight into the catalytic residues, substrate binding, and the effects of mutations. In particular, the structure of the Y206A mutant helps to explain the higher ratio of the rates of synthesis and hydrolysis that this mutant displays.

## EXPERIMENTAL PROCEDURES

*Protein Production*—Plasmids, bacterial strains, growth conditions, and purification methods for the production of native, S205A, and Y206A *A. turbidans* AEH with a C-terminal *myc* epitope and His tag were as described in Ref. 6. Briefly, proteins were produced in *Escherichia coli* TOP10 cells carrying constructs derived from pBAD. Cells were grown at 14 °C for 4 days in LB medium with 100 μg/ml ampicillin and 0.01% (w/v) arabinose for induction. After harvesting and washing, cells were either sonicated or passed through a French press and a clear lysate was prepared by centrifugation. AEH and mutant AEHs were purified from this lysate by metal ion affinity chromatography using nickel-nitrilotriacetic acid-agarose (Qiagen). A stepwise gradient of 50–200 mM imidazole in 150 mM NaCl, 50 mM sodium phosphate, pH 7.4, was used for elution. Pure protein eluted around 75–100 mM imidazole. Subsequently, the protein was desalted using gel filtration. Determination of the oligomeric state was carried out by gel filtration on a Superdex 200 column equilibrated with 50 mM sodium phosphate buffer, pH 6.2, containing 200 mM sodium chloride. Elution volumes were calibrated using Bio-Rad gel filtration markers.

*Determination of Kinetic Parameters*—For the determination of enzyme behavior in a cephalexin synthesis reaction, the enzymes were incubated with 15 mM D-phenylglycine methyl ester (D-PGM) and 30 mM β-lactam nucleus 7-amino-desacetoxycephalosporanic acid in 50 mM Na-phosphate buffer, pH 6.2, at 30 °C. Kinetic parameters for cephalexin hydrolysis were previously reported in Ref. 6 and are given here for reference. The synthesis of cephalexin and the hydrolysis of D-PGM were followed by high performance liquid chromatography as described before (4). Enzymes were used at a concentration that catalyzed the hydrolysis of D-PGM with an initial rate of 0.20 to 0.30 mM/min. To obtain the rate of enzymatic D-phenylglycine production, the observed rate of D-phenylglycine production was corrected for the first-order chemical hydrolysis of D-PGM. The relative rate of antibiotic formation *versus* hydrolysis of D-PGM ($V_s/V_h^{ini}$) was determined from the initial slope of antibiotic formation divided by the rate of enzymatic formation of the hydrolysis product (D-phenylglycine). The rates were measured at less than 10% conversion of D-PGM to minimize the influence of product hydrolysis. The kinetic parameters $K_m$ and $k_{cat}$ were calculated using nonlinear regression fitting (Scientist, Micromath) with Michaelis-Menten and substrate inhibition kinetics. The calculated parameters are given with their standard deviations. The maximum product concentration ($P_S^{max}$) was determined by following the concentrations of cephalexin and D-phenylglycine over time, until the product concentration started to decrease. All measurements were at least performed in duplicate.

*Crystal Preparation*—His-tagged native and mutant AEHs were concentrated to 5 mg/ml by ultrafiltration. WT *A. turbidans* AEH and the Y206A mutant were crystallized by mixing 3 μl of protein solution with 3 μl of 15–17% PEG 4000, 0.2 M ammonium acetate, 0.1 M sodium acetate buffer, pH 4.6, followed by equilibration against this PEG solution. Prism-shaped crystals of WT protein of maximum dimensions 0.2 × 0.05 × 0.05 mm were obtained in 1 week. Plate-shaped crystals (0.2 × 0.2 × 0.01 mm) of the Y206A mutant were obtained in 4 days. In an attempt to obtain a complex with a substrate, WT crystals were transferred to mother liquor containing 10 mg/ml ampicillin for 30 min after which they were cryoprotected by soaking for a few seconds in the

**TABLE 1**

**Data collection and refinement statistics**

Where applicable, values for the highest resolution shell are given in parentheses.

| Data collections | WT | WT-D-phenylglycine | S205A-ampicillin | Y206A |
|---|---|---|---|---|
| **Statistics** | | | | |
| Protein Data Bank code | 2B9V | 2B4K | 1NX9 | 1RYY |
| Wavelength (Å) | 0.933 | 0.934 | 0.8463 | 0.9393 |
| Space group and cell dimensions | $P2_1$, $a$ = 98.4, $b$ = 275.6, $c$ = 197.0 Å, $\beta$ = 90.1° | $I23$, $a = b = c$ = 341.0 Å, $\alpha = \beta = \gamma$ = 90° | $I23$, $a = b = c$ = 341.8 Å, $\alpha = \beta = \gamma$ = 90° | $P2_1$, $a$ = 91.6, $b$ = 177.5, $c$ = 170.0 Å, $\beta$ = 91.0° |
| Resolution range (Å) | 40–2.0 | 40–3.0[a] | 99–2.2 | 40–2.8 |
| No. of unique reflections | 598,744 | 121,384 | 322,911 | 134,932 |
| Completeness (%) | 85.5 (67.8) | 93.2 (91.5) | 97.2 (84.3) | 99.4 (99.6) |
| Redundancy | 2.8 | 2.6 | 4.5 | 3.2 |
| $R_{sym}$ | 0.091 (0.341) | 0.186 (0.917) | 0.081 (0.322) | 0.066 (0.184) |
| $I/\sigma$ | 6.6 (1.5) | 7.1 (2.8) | 14.3 (3.7) | 17.2 (6.9) |
| **Refinement statistics** | | | | |
| Residue range in refinement (Å) | 40–2.0[b] | 15–3.3 | 15–2.2 | 40–2.8 |
| No. reflections in refinement | 504,379 | 91,758 | 304,675 | 125,967 |
| Protein atoms | 77,072 | 19,536 | 19,532 | 39,016 |
| Water molecules | 3,654 | 6 | 2,229 | 0 |
| Ligand atoms | | D-Phenylglycine, 33 (3 molecules); glycerol, 18 (3 molecules) | Ampicillin, 96 (4 molecules); glycerol, 24 (4 molecules) | 0 |
| $R$-factor | 0.199 | 0.258 | 0.166 | 0.253 |
| $R_{free}$ | 0.235 | 0.289 | 0.184 | 0.272 |
| **Root mean square deviations from ideal geometry** | | | | |
| Bonds (Å) | 0.008 | 0.009 | 0.007 | 0.009 |
| Angles (°) | 1.7 | 1.0 | 1.1 | 0.8 |
| **Ramachandran plot** | | | | |
| Most favored | 87.0% | 82.7% | 86.0% | 84.1% |
| Additional allowed | 12.6% | 17.1% | 13.6% | 15.4% |
| Disallowed (these include catalytic and structurally important residues) | 0.3% | 0.2% | 0.4% | 0.4% |

[a] Due to the high merging $R$-factor at 3.0-Å resolution, only data to 3.3-Å resolution were used for refinement.

[b] The data used for the refinement of the WT structure are only 75% complete due to collection geometry and detwinning; however, the number of reflections used in the refinement of this structure corresponds to the number of reflections in a 100% complete dataset to 2.2-Å resolution.

same solution containing 25% glycerol, and cryocooled in liquid nitrogen. Y206A crystals were subjected to the same procedure, substituting D-phenylglycine methyl ester for ampicillin. Crystals of a S205A mutant-ampicillin complex were grown by mixing 3 μl of protein solution with 3 μl of a reservoir solution containing 0.3 M sodium citrate buffer, pH 5.6, 13–14% PEG 4000, and 10 mM sodium ampicillin, followed by equilibration in hanging drops against 500 μl of this latter solution for 3–4 days. Rhombic dodecahedra with a size of 0.3 × 0.3 × 0.3 mm were harvested and cryocooled after soaking for 30 s in reservoir solution containing 26% glycerol. WT·D-phenylglycine complex crystals were grown in the same way, substituting WT protein for the mutant and D-phenylglycine for ampicillin. All crystallization and soaking experiments were carried out at room temperature.

*Data Collection and Structure Solution*—Useful diffraction data from WT, WT·D-phenylglycine, and Y206A crystals were collected to 2.0-, 3.3-, and 2.8-Å resolution, respectively, on beam line ID14-4 at the ESRF in Grenoble, France. Diffraction data from crystals of the S205A mutant co-crystallized with ampicillin were collected to 2.2-Å resolution on the BW7B beam line of the EMBL outstation at the DESY synchrotron in Hamburg, Germany. All data were processed with DENZO and SCALEPACK (17). The structure of the *A. turbidans* AEH was solved by molecular replacement, using the program AMoRe (18) and the previously determined tetrameric structure of the *X. citri* AEH as a search model. The structure determination of the WT protein was hampered by twinning in combination with pseudo-crystallographic translation symmetry, and the structure elucidation process followed with this protein is further described in Ref. 19. Briefly, a high twinning fraction was observed, which made it impossible to detwin the data mathematically. Therefore, the twinning was idealized by averaging intensities of twin-related reflections (20) and the structure of the one twin domain, solved by molecular replacement, was used to obtain detwinned intensities for refinement. It should be noted, that because the measured data are relatively incomplete (85.5% completeness), not all twin-related reflection pairs could be averaged for lack of availability of one of the reflections. After averaging and detwinning, this leads to the availability of only 75% of all possible reflections for refinement. However, this number of available reflections corresponds to the number of reflections that a 100% complete dataset of 2.2-Å resolution from this crystal would have, thus effectively limiting the resolution to ~2.2 Å. The twinning also results in the loss of independence of twin-related reflections, lowering the observation/parameter ratio further. However, there are 16 AEH monomers in the asymmetric unit (four AEH tetramers), enabling the use of tight 16-fold non-crystallographic symmetry restraints, which ensures that the refinement problem is sufficiently well determined.

Final models of all proteins were obtained through iterative cycles of refinement with Refmac 5.0 (21), combined with rebuilding in Xfit (22). During refinement of the Y206A mutant structure, 8-fold non-crystallographic symmetry restraints were employed. Data collection and refinement parameters are given in Table 1.

## RESULTS AND DISCUSSION

*Native Structure: Oligomeric State*—The structures of the WT, WT·D-phenylglycine, Y206A, and S205A AEH were successfully determined by x-ray crystallography. Despite different space groups and crystallization conditions, all structures showed the same tetrameric arrangement of monomers (Fig. 2*a*), which was also observed for the *X.*

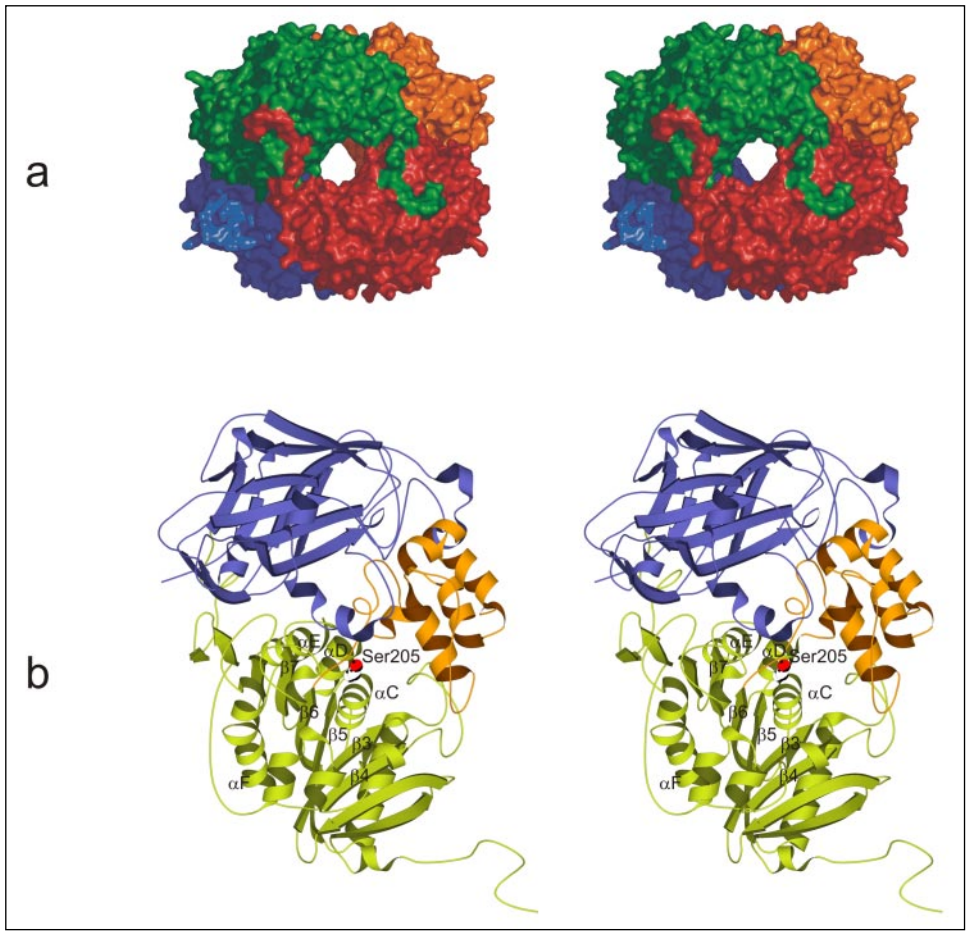


FIGURE 2. *a*, stereo figure of the *A. turbidans* α-amino acid ester hydrolase tetramer. A surface representation is shown, in which each monomer is individually colored. *b*, stereo figure of the *A. turbidans* α-amino acid ester hydrolase monomer. The arm and α/β-hydrolase domains are shown in *green*, the cap domain in *orange*, and the jellyroll domain in *blue*. The side chain of the active site $Ser^{205}$ is shown in space filling representation. Helices αC–αF and strands β4–β7 are labeled. The figure was prepared using PYMOL (DeLano Scientific) and Molscript (30).

*citri* AEH (7). Gel filtration experiments with the WT protein and the S205A mutant indicated the presence of exclusively tetramers in solution, reinforcing the notion that the crystallographically observed tetramer represents the physiological oligomerization state.

The *Acetobacter* AEH tetramer (Fig. 2*a*) has the shape of a hollow sphere with a diameter of about 100 Å. The central cavity can only be reached through two diametrically opposed entrances that are each ~15 Å wide. Because the active sites are found on the inside of the sphere, this tetrameric oligomerization state would restrict the AEHs to converting small compounds.

The native structure of the *Acetobacter* AEH monomer (Fig. 2*b*) resembles that of the *Xanthomonas* AEH monomer. It can be superimposed with *Xanthomonas* AEH to within a root mean square difference of Cα positions of 4.5 Å. Like the *Xanthomonas* enzyme, it includes an N-terminal arm, an α/β-hydrolase domain with a helical cap domain, and a C-terminal jellyroll fold domain. The N-terminal arm consists of 24 residues that form an elongated polypeptide that interacts with the surface of another monomer. Residues 62–73, in the middle of the arm, could not be identified in the electron density map. These residues span the gap between the two monomers held together by the arm, and may thus be expected to be mobile, because they make no non-bonded contacts with either monomer. However, their approximate positions can be inferred from the short distance between the beginning and end of this gap and their better defined positions in the S205A mutant structure.

The arm is followed by a typical α/β-hydrolase fold domain, consisting of a highly twisted β-sheet flanked on both sides by α-helices (23–25). Apart from the second one, all strands in the sheet are parallel. Adopting the nomenclature in Ref. 23, the catalytic residues $Ser^{205}$, $His^{370}$, and $Asp^{338}$ are found at their canonical positions on the loops between strand β5 and helix αC, between β8 and αF, and between β7 and αE, respectively. Compared with the classical α/β-hydrolase fold, which has eight β-strands in the central sheet, AEH displays two additional β-strands at the C terminus of the domain. Furthermore, several insertions are seen, most notably a predominantly helical cap domain between β6 and αD. Another insertion between β3 and αA contains the conserved $Tyr^{112}$, which is in a position to contribute with its hydroxyl group to oxyanion stabilization during the reaction. The C-terminal domain adopts a jellyroll fold with several insertions, one of which contains a helix that approaches the active site as in the *X. citri* AEH.

*Active Site Structure*—The active site is found at the interface of the α/β-hydrolase, cap, and jellyroll domains. The catalytic $Ser^{205}$ is located on the so-called nucleophile elbow between β5 and αC and has unfavorable main chain dihedrals as is usual in α/β-hydrolase family members (25). It is closely approached by $His^{370}$, which in turn is hydrogen bonded to $Asp^{338}$. Thus, a canonical Ser-His-Asp catalytic triad is formed. The backbone amide of $Tyr^{206}$, which directly follows the catalytic serine in the sequence, and the phenolic OH of the $Tyr^{112}$ side chain form an oxyanion hole similar to that observed in *X. citri* AEH, CocE, and PepX (7–9). As in these proteins, $Tyr^{112}$ makes stacking-like interactions with the $Pro^{111}$ ring, as does $Tyr^{206}$ on the other side of the $Pro^{111}$ side chain (figure 3*a*). The $Tyr^{112}$ side chain is further restrained by a hydrogen bond with the $Tyr^{253}$ side chain (not shown).

Close to the active serine, a pocket is present, delineated by residues stemming mostly from the cap domain. It is found in the position were the acyl chain would be expected in an acyl-enzyme compound. In a

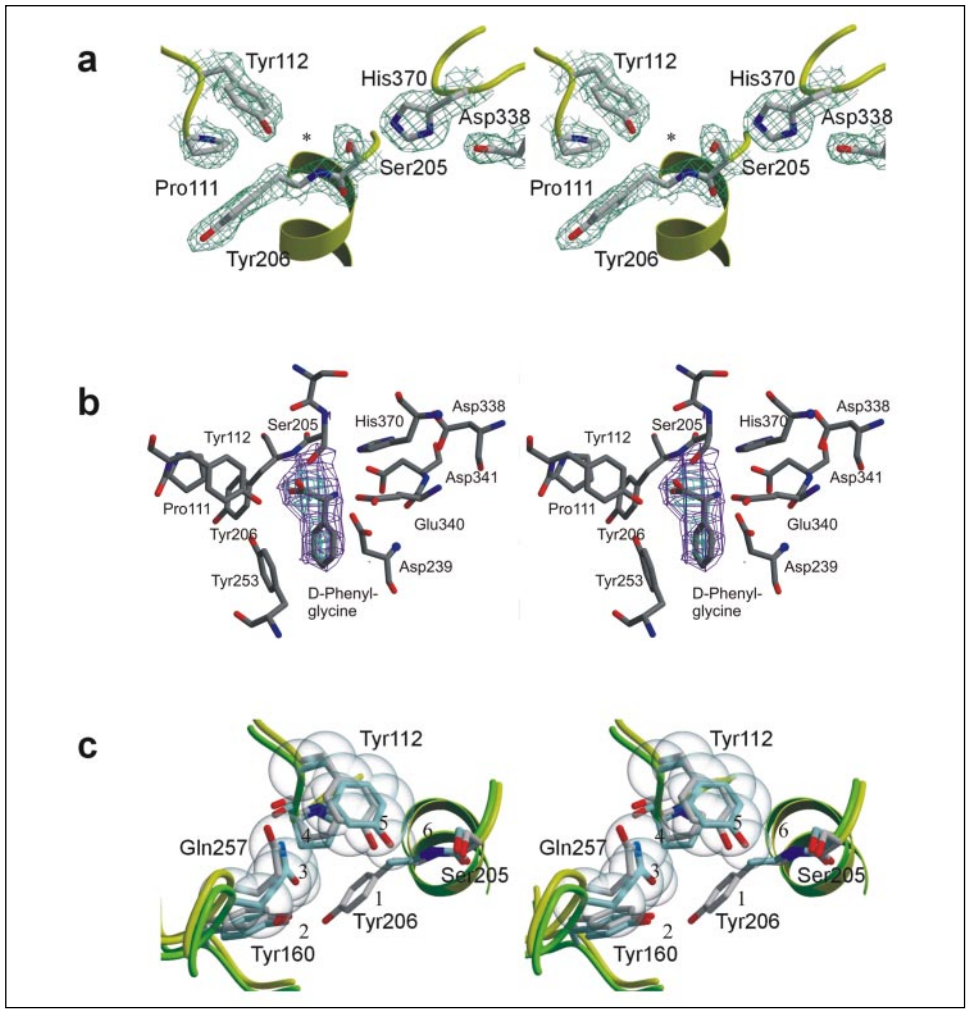


FIGURE 3. *a*, stereo figure showing the active site residues of *A. turbidans* AEH. The catalytic triad and the residues forming the oxyanion hole are shown in *stick* representation. An *asterisk* indicates the expected position of the oxyanion hole. The $2F_o - F_c$ electron density map is overlaid on the structure at a 1.0-$\sigma$ contour level. *b*, stereo figure, showing ($F_o - F_c$) difference electron density calculated with the D-phenylglycine co-crystal data prior to including D-phenylglycine in the model, overlaid on the refined D-phenylglycine complex structure. The ammonium group of D-phenylglycine is in close proximity to the carboxylate cluster. *c*, stereo figure comparing the active site residues of WT (*gray*) and Y206A (*blue*) AEH. Transparent spheres indicate the van der Waals radii of the atoms of the interacting $Tyr^{112}$ and $Asn^{257}$ residues in the Y206A structure. The changes upon the mutation of $Tyr^{206}$ to Ala are indicated with numbers: *1*, mutation of $Tyr^{206}$ to Ala; *2*, loss of the hydrogen bond with $Tyr^{160}$; *3*, movement of the $Gln^{257}$ side chain; *4*, van der Waals interactions of $Gln^{257}$ side chain with $Tyr^{112}$ side chain; *5*, movement of $Tyr^{112}$ side chain toward oxyanion hole; *6*, possible hydrogen bond between $Tyr^{112}$ O$\eta$ and $Ser^{205}$ O$\gamma$. The figure was prepared using Xfit (22), BobScript (31), and Raster3D (32).

difference Fourier synthesis using data collected from an AEH crystal grown in the presence of D-phenylglycine, strong difference density was observed in three of four active sites of the tetramer, consistent with D-phenylglycine binding to this site, again pointing to this pocket being the acyl chain binding site (Fig. 3*b*). In the complex, the aromatic ring of phenylglycine makes stacking interactions with $Tyr^{253}$. On the other side of the catalytic serine, a much larger space is observed, which could accommodate a bulky leaving group during the enzyme acylation step of the reaction, and could bind a large acyl acceptor during the enzyme deacylation step.

*Substrate Specificity*—On one side of the putative acyl binding pocket, a cluster of acidic residues was observed (Fig. 3*b*). These residues ($Asp^{239}$, $Glu^{340}$, and $Asp^{341}$) form the conserved cluster proposed to recognize the α-amino group of the substrate (7) and can be superimposed with the corresponding residues of the *X. citri* AEH to a root mean square deviation of 0.88 Å. In the difference electron density observed in the AEH·D-phenylglycine complex, D-phenylglycine could be placed with its ammonium group close to the acidic residues (Fig. 3*b*).

Interestingly, despite the presence of a canonical catalytic triad, compounds that lack an α-amino group are not normally converted. Also, AEH is not inhibited by the neutral reagent phenylmethanesulfonyl fluoride, but it is inhibited by *p*-nitrophenyl-p′-guanidinobenzoate (6), which carries a positive charge in solution at neutral pH. These observations can be explained in two ways. First, the binding of a neutral substrate would bury the three carboxylate groups of the cluster without neutralizing their negative charge, which would be energetically unfavorable. Second, the distance between the $Asp^{239}$ Oδ and the catalytic $Ser^{205}$ Oγ is only 3.5 Å. The close proximity of the negatively charged $Asp^{239}$ Oδ would severely decrease the nucleophilicity of $Ser^{205}$ Oγ by inhibiting its deprotonation by the catalytic His/Asp combination, thereby precluding the acylation reaction unless the charge of $Asp^{239}$ is compensated by a positive amino group on the substrate. These effects would also explain why AEHs convert esters of phenylglycine, but are not inhibited by phenyl acetic acid, which differs from phenylglycine only in the absence of the α-amino group.

*Effects of Mutations*—Previously, several important residues in AEH were identified by site-directed mutagenesis. Specifically, the influence of mutation of the G*X*S*Y*X*G* consensus motif was investigated, which helped to identify the catalytic serine 205. Mutation of this residue almost completely abolished activity (4, 6). The crystal structure of the S205A mutant shows no appreciable differences in side or main chain conformations in the active site compared with the native enzyme. Thus, its inactivity is solely because of the loss of the $Ser^{205}$ hydroxyl group.

As mentioned above, previous work identified $Tyr^{206}$ as a candidate for mutation in the development of AEH mutants with improved biocatalytic properties. Kinetic parameters for the wild-type enzyme and the Y206A mutant were determined and are reported in Table 2. Compared with wild-type enzyme, the Y206A mutant shows a reduced $k_{cat}$ toward both cephalexin and D-phenylglycine methyl ester. Furthermore, it displays a 3-fold increase in the ratio of the initial rates of

**TABLE 2**

**Kinetic properties of WT and Y206A AEH**

Kinetic parameters for cephalexin hydrolysis, D-phenylglycine methylester (D-PGM) hydrolysis, with the specificity ratio $\alpha$, and the ratio of the initial rates of synthesis and hydrolysis $V_s/V_h^{ini}$ and maximum product concentration $P_S^{max}$ in a kinetically controlled cephalexin synthesis reaction.

| | D-PGM hydrolysis | | | Cephalexin hydrolysis (from Ref. 6) | | | Cephalexin synthesis from D-PGM/7-ADCA[a] | | |
|---|---|---|---|---|---|---|---|---|---|
| | $k_{cat}$ | $K_m$ | $k_{cat}/K_m$ | $k_{cat}$ | $K_m$ | $k_{cat}/K_m$ | $\alpha$ | $V_s/V_h^{ini}$ | $P_s^{max}$ |
| | $s^{-1}$ | mM | | $s^{-1}$ | mM | $s^{-1}mM^{-1}$ | | | mM |
| WT | 1067 ± 56 | 1 ± 0.1 | 1067 ± 121 | 274 ± 7 | 0.45 ± 0.06 | 609 ± 83 | 0.6 | 2.4 ± 0.8 | 5.4 ± 0.1 |
| Y206A | 655 ± 39 | 5.3 ± 0.9 | 124 ± 22 | 120 ± 2 | 4.0 ± 0.2 | 30 ± 2 | 0.24 | 9 ± 2 | 8.6 ± 0.6 |

[a] 7-ADCA, 7-amino-desacetoxycephalosporanic acid.

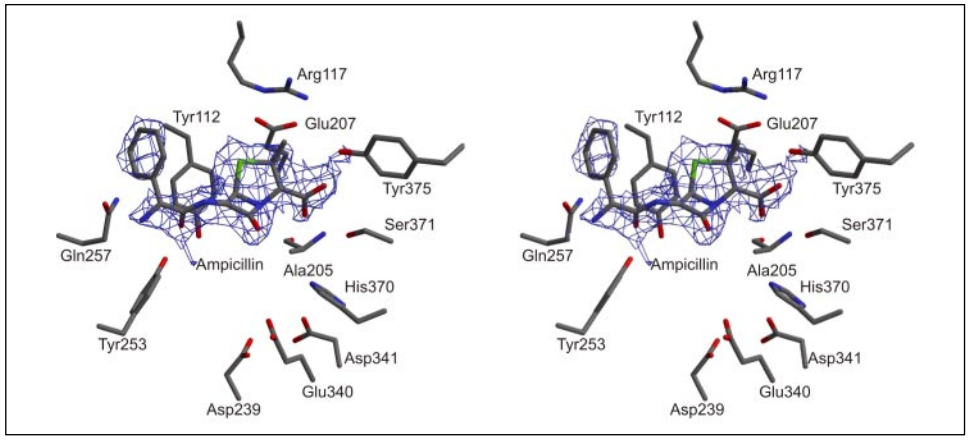


FIGURE 4. **Stereo picture of the $2F_o - F_c$ electron density of ampicillin in the active site of the S205A mutant, after refinement of the initial molecular replacement solution, prior to inclusion of ampicillin in the model.** The density was contoured at 1.0 $\sigma$, and overlaid on the final refined structure. The figure was prepared using Xfit (22) and Raster3D (32).

synthesis and hydrolysis ($V_s/V_h^{ini}$ during cephalexin synthesis as well as a ~60% increase in maximum cephalexin accumulation.

$Tyr^{206}$ is part of the so-called nucleophile elbow and is believed to stabilize the oxyanion of the tetrahedral transition state with its backbone amide (7), whereas its side chain points into the protein, away from the active site cavity. However, the backbone conformations of the nucleophilic elbows of the wild-type and Y206A proteins show no large differences. Thus, the altered catalytic properties of this mutant are difficult to explain through a direct effect of the Tyr to Ala mutation. They can, however, be explained by indirect effects on the local structure (see Fig. 3*c*). In the native structure, the buried $Tyr^{206}$ side chain forms a hydrogen bond with another buried tyrosine, $Tyr^{160}$. In the Y206A mutant, the loss of the hydrogen bonding partner of $Tyr^{160}$ is compensated for by a rearrangement of $Gln^{257}$ on the surface of the protein. A ~180° rotation around the $C_\gamma$-$C_\delta$ bond, and an ~80° rotation around the $C_\beta$-$C_\gamma$ bond point the $Gln^{257}$ O$\epsilon$-1 atom into the protein, where it hydrogen bonds with the buried $Tyr^{160}$. However, in the wild-type structure the $Gln^{257}$ side chain is in close proximity to the side chain of $Tyr^{112}$, which is believed to contribute to stabilizing the oxyanion developing during catalysis (7). In the mutant, the rearrangement of the $Gln^{257}$ side chain causes a significant shift of the $Tyr^{112}$ side chain toward the catalytic serine (see Fig. 3*c*). Thus, the distance between the $Tyr^{112}$ O$\eta$ and the reactive $Ser^{205}$ O$\gamma$ becomes on average 3.4 Å in the mutant, corresponding to a weak hydrogen bond, whereas in the wild-type enzyme, this distance is on average 4.5 Å. The close interaction in the mutant will lower the nucleophilicity of the serine O$\gamma$, rendering it less reactive, which would explain the reduced $k_{cat}$ values of the Y206A mutant enzyme. Additionally, the observed decrease in activity can be explained by a less favorable positioning of the $Tyr^{112}$ hydroxyl group for transition state stabilization. In either case, the mutation of one of the two oxyanion hole-forming residues perturbs the position of the other, thus affecting the properties of the oxyanion hole indirectly.

The explanation of the increase in the ratio of the initial rates of synthesis and hydrolysis ($V_s/V_h^{ini}$) during cephalexin synthesis is less straightforward. Apparently, the mutation affects the interaction of the acyl enzyme with the competing nucleophilic acyl acceptors, water and the $\beta$-lactam nucleus, by altering the way in which the acyl enzyme is presented to an acyl acceptor, or the way in which the acceptor is bound and/or activated. Possibly, the geometry of the atoms around the scissile bond between enzyme and acyl group is changed to favor attack by a $\beta$-lactam rather than by water (26). An alternative explanation is that $Tyr^{112}$ participates directly in binding the acceptor, in which case a change in the position of $Tyr^{112}$ could affect both binding affinity and binding mode.

Indeed, the $Tyr^{112}$ phenol ring is part of the surface of the site where the $\beta$-lactam part of the product would be expected to bind. The involvement of $Tyr^{112}$ in $\beta$-lactam binding has been proposed for the *X. citri* AEH (7). Interestingly, in the homologous PepX (9), the corresponding residue is in the middle of a large hydrophobic patch on the surface of the active site, and could thus play a role in substrate binding in this case as well. The corresponding tyrosine in the homologous CocE has been proposed to interact with the leaving group part of the substrate in cocaine hydrolysis, too (27). Participation of this tyrosine residue in substrate binding would mean that it plays a dual role in that apart from oxyanion stabilization through the main chain amide, its side chain also interacts with a different part of the substrate, at other stages in the reaction.

The higher maximum product accumulation in antibiotic synthesis by the Y206A mutant has been attributed to a decrease in the affinity of the enzyme for the antibiotic (6, 16). This, too, could be caused by an altered positioning of $Tyr^{112}$ influencing its affinity for a $\beta$-lactam.

*Ampicillin Binding Mode*—Crystals of the inactive S205A mutant were grown in the presence of ampicillin, and $F_o - F_c$ and $2F_o - F_c$ maps calculated after refinement of the initial molecular replacement solution showed an ampicillin molecule bound in the active site of each mono-

mer. The antibiotic predominantly makes hydrophobic contacts with $Tyr^{112}$, both with its acyl chain and its β-lactam moiety (Fig. 4). Additional interactions are made with $Tyr^{375}$, $Ser^{371}$, $Arg^{117}$, and $Glu^{207}$. The carbon atom of the scissile amide bond is ~10 Å away from the $Ala^{205}$ Cα, indicating that in the native protein, attack by $Ser^{205}$ would not be possible in this binding mode. Perhaps, the non-productive binding mode of ampicillin in the AEH active site is caused by the high glycerol concentration used to cryoprotect the crystal. Electron density compatible with a glycerol molecule is observed in the putative acyl binding pocket, suggesting that the glycerol has displaced the ampicillin from its productive binding site into the position observed. Although ampicillin does not bind in a productive mode in the S205A structure, this result does show the propensity of $Tyr^{112}$ for ligand binding.

*Conclusions and Outlook*—The structure determination of the *A. turbidans* α-amino acid ester hydrolase and of two mutants has resulted in a view of an active site that combines a classical catalytic triad with unusual elements like a cluster of acidic residues and an oxyanion hole with a tyrosine side chain contribution. In detail, the structures show how mutation of $Tyr^{206}$ to alanine results in a shift in position of $Tyr^{112}$, altering both the oxyanion hole and the surface of the leaving group binding pocket. Given the effects of this mutation on the synthesis/hydrolysis ratio and the binding of antibiotics, this result points to a function for $Tyr^{112}$ in leaving group/acceptor binding next to its proposed function in oxyanion stabilization.

Additional research focused on improving the catalytic properties of AEHs could be directed toward understanding the molecular details of the hydrolysis reaction. Papers describing both crystallographic (28) and simulation (29) studies of serine proteases have suggested that in such enzymes the attacking water molecule is first bound to the protein in a position close to the acyl enzyme ester bond and the catalytic histidine. It is then activated by the histidine, and attacks the ester bond. Looking at candidate "landing platforms" for such a water molecule in the AEH structures yields a position close to $Ser^{371}$. In five of the 16 monomers in the wild-type structure, a water molecule is observed hydrogen bonded to the $Ser^{371}$ side chain, close to the catalytic histidine Nε-2, by which it could be activated for attack. In the *A. turbidans* AEH S205A-ampicillin complex, this position is occupied by an oxygen atom of ampicillin. In the *X. citri* AEH structure, a water molecule was observed in the corresponding position, too. Identifying a hydrolytic water molecule in AEH might allow additional mutations to be made that reduce the hydrolysis rate and lead to even better catalytic properties.

*Acknowledgments—We thank Dr. Jan-Metske van der Laan (DSM food specialties) for a fruitful cooperation and the ESRF in Grenoble and the EMBL outstation in Hamburg for synchrotron beam time. Drs. Ehmke Pohl and Cristofer Enroth are gratefully acknowledged for assistance with data collection.*

**REFERENCES**

1. Takahashi, T., Yamazaki, Y., Kato, K., and Isona, M. (1972) *J. Am. Chem. Soc.* **94,** 4035–4037
2. Bruggink, A., Roos, E. C., and de Vroom, E. (1998) *Org. Process Res. Dev.* **2,** 128–133
3. Takahashi, T., Yamazaki, Y., and Kato, K. (1974) *Biochem. J.* **137,** 497–503
4. Polderman-Tijmes, J. J., Jekel, P. A., de Vries, E. J., van Merode, A. E. J., Floris, R., van der Laan, J. M., Sonke, T., and Janssen, D. B. (2002) *Appl. Env. Microbiol.* **68,** 211–218
5. Chich, J.-F., Chapot-Chartier, M.-P., Ribadeau-Dumas, B., and Gripon, J.-C. (1992) *FEBS Lett.* **314,** 139–142
6. Polderman-Tijmes, J. J., Jekel, P. A., Jeronimus-Stratingh, C. M., Bruins, A. P., van der Laan, J. M., Sonke, T., and Janssen, D. B. (2002) *J. Biol. Chem.* **277,** 28474–28482
7. Barends, T. R. M., Polderman-Tijmes, J. J., Jekel, P. A., Hensgens, C. M. H., de Vries, E. J., Janssen, D. B., and Dijkstra, B. W. (2003) *J. Biol. Chem.* **278,** 23076–23084
8. Larsen, N. A., Turner, J. M., Stevens, J., Rosser, S. J., Basran, A., Lerner, R. A., Bruce, N. C., and Wilson, I. A. (2001) *Nat. Struct. Biol.* **9,** 17–21
9. Rigolet, P., Mechin, I., Delage, M.-M., and Chich, J.-F. (2002) *Struct. Fold. Des.* **10,** 1383–1394
10. Kato, K. (1980) *Agric. Biol. Chem.* **44,** 1083–1088
11. Nam, D. H., Kim, C., and Ryu, D. D. Y. (1985) *Biotech. Bioeng.* **27,** 953–960
12. Blinkovsky, A. M., and Markaryan, A. N. (1993) *Enzyme Microb. Technol.* **15,** 965–973
13. Fernandez-Lafuente, R., Hernández-Justiz, O., Mateo, C., Terreni, M., Alonso, J., Garcia-López, J. L., Moreno, M. A., and Guisan, J. M. (2001) *J. Mol. Catal. B. Enz.* **11,** 633–638
14. Youshko, M. I., Chilov, G. G., Shcherbakova, T. A., and Svedas, V. K. (2002) *Biochim. Biophys. Acta* **1599,** 134–140
15. Alkema, W. B. L. (2002) *Faculty of Mathematics and Natural Sciences*, Ph.D. thesis, pp. 142, University of Groningen, Groningen
16. van der Laan, J. M., Polderman-Tijmes, J. J., and Barends, T. R. M. (2002) International Patent Application WO 02/086111 A2
17. Otwinowksi, Z., and Minor, W. (1997) *Methods Enzymol.* **276,** 307–326
18. Navaza, J. (1994) *Acta Crystallogr. Sect. A Crystallogr.* **50,** 157–163
19. Barends, T. R. M., and Dijkstra, B. W. (2003) *Acta Crystallogr. Sect. D Biol. Crystallogr.* **59,** 2237–2241
20. Yeates, T. O. (1997) *Methods Enzymol.* **276,** 344–358
21. Murshudov, G. N., Vagin, A. A., and Dodson, E. J. (1997) *Acta Crystallogr. Sect. D Biol. Crystallogr.* **53,** 240–255
22. McRee, D. E. (1999) *J. Struct. Biol.* **125,** 156–165
23. Ollis, D. L., Cheah, E., Cygler, M., Dijkstra, B., Frolow, F., Franken, S. M., Harel, M., Remington, S. J., Silman, I., Schrag, J., Sussman, J. L., Verschueren, K. H. G., and Goldman, A. (1992) *Protein Eng.* **5,** 197–211
24. Heikinheimo, P., Goldman, A., Jeffries, C., and Ollis, D. L. (1999) *Struct. Fold Des.* **7,** R141-R146
25. Nardini, M., and Dijkstra, B. W. (1999) *Curr. Opin. Struct. Biol.* **9,** 732–737
26. Alkema, W. B. L., Dijkhuis, A. J., de Vries, E., and Janssen, D. B. (2002) *Eur. J. Biochem.* **269,** 2093–2100
27. Turner, J. M., Larsen, N. A., Bashan, A., Barbas, C. F., Bruce, N. C., Wilson, I. A., and Lerner, R. A. (2002) *Biochemistry* **41,** 12297–12307
28. Singer, P. T., Smalas, A., Carty, R. P., Mangel, F. W., and Sweet, R. M. (1993) *Science* **261,** 620–622
29. Topf, M., Várnai, P., Schofield, C., and Richards, W. G. (2002) *Protein Struct. Funct. Genet.* **47,** 357–369
30. Kraulis, P. (1991) *J. Appl. Crystallogr.* **24,** 946–950
31. Esnouf, R. M. (1997) *J. Mol. Graph.* **15,** 133–138
32. Merritt, E. A., and Bacon, D. J. (1997) *Methods Enzymol.* **277,** 505–524